Relating arctic pack ice stress and deformation under winter conditions

Jacqueline A. Richter-Menge,[1] S. Lyn McNutt,[2] James E. Overland,[3] and Ronald Kwok[4]

Received 5 June 2000; revised 2 April 2001; accepted 12 September 2001; published 27 September 2002.

[1] Together, thermodynamic and dynamic processes determine the thickness distribution of the ice cover on polar oceans, which governs the exchange of energy between the atmosphere and the ocean. Key to the dynamic processes is the mechanical behavior of the ice cover. During the Surface Heat Budget of the Arctic Ocean (SHEBA) field experiment, we deployed sensors to measure the internal ice stress at several locations within a 15 × 15 km area. These measurements are combined with satellite-derived ice motion and imagery products. The objective is to make a first step toward using these data sources for evaluating sea ice dynamics models by assessing whether the stress signal can be qualitatively linked to the regional-scale (10–100 km) deformation activity. Four case studies are presented, each with distinguishing characteristics: consolidation of the seasonal ice zone against the Alaskan coast (5–7 December 1997); advancement of the consolidation zone into the perennial ice pack (11–13 December); extreme divergence (14–17 January); and consolidation of the pack against Wrangel Island and the Siberian coast (20–23 February). The results of this analysis (1) demonstrate that stress measurements are related to the regional deformation behavior of the ice cover, (2) confirm that regional-scale ice dynamics is primarily a function of coastal geometry and sustained, large-scale wind direction and magnitude, (3) provide continued evidence that the ice pack behaves as a granular hardening plastic, and (4) encourage pursuit of efforts to use direct measurements of ice stress and deformation in the formulation and development of sea ice dynamics models. *INDEX TERMS:* 4540 Oceanography: Physical: Ice mechanics and air/sea/ice exchange processes; 4207 Oceanography: General: Arctic and Antarctic oceanography; *KEYWORDS:* sea ice, stress, deformation, remote sensing

Citation: Richter-Menge, J. A., S. L. McNutt, J. E. Overland, and R. Kwok, Relating arctic pack ice stress and deformation under winter conditions, *J. Geophys. Res.*, *107*(C10), 8040, doi:10.1029/2000JC000477, 2002.

1. Introduction

[2] The role of the polar oceans in the global climate system is an important consideration in the development of general circulation models (GCMs). Unique to these oceans is their ice cover, which is characterized by extreme spatial and temporal variability. The presence of the ice cover and its evolution significantly affect the heat exchange between the ocean and atmosphere. It is well known that the sea ice cover acts as a thermal insulator between the ocean and the atmosphere [*Untersteiner*, 1961; *Maykut and Untersteiner*, 1971]. The energy exchange characteristics of this insulating layer depend in large part on its thickness. Using a simple model of heat transport through the sea ice, *Maykut* [1978] found that during the winter months the net heat flux to the atmosphere from ice less than 0.4 m thick is 1–2 orders of magnitude greater than from thicker perennial ice. The thickness distribution of the sea ice cover is determined by its combined thermodynamic and dynamic history [*Thorndike et al.*, 1975]. Thermodynamic processes dictate the growth and ablation of the ice. Motion of the ice, in response to wind and current forcing, results in the formation of both leads and ridges, which create areas of thinner and thicker ice, respectively.

[3] GCM simulations have shown that arctic processes affect climate change predictions of warming, but that model results vary significantly depending on how the sea ice cover is represented [*Washington and Meehl*, 1986; *Pollard and Thompson*, 1994; *Rind et al.*, 1995]. A common conclusion of these investigations is that sea ice processes need to be realistically represented in the coupled models if their predictions are to be considered with any confidence. Comparisons of thermodynamic-only and dynamic-thermodynamic model results consistently indicate that when the dynamics are included, the sensitivity of the arctic environment to temperature perturbations is reduced [*Hibler*, 1984; *Holland et al.*, 1993; *Pollard and Thompson*, 1994; *Arbetter et al.*, 1997]. This is due, in part, to a negative feedback between ice thickness and ice strength. As ice thins because of warming, its strength decreases, resulting in more extensive deformation and, hence, thickening.

[4] In the coupled models that consider the effects of ice dynamics, the sea ice model commonly adopted is that

[1]CRREL-ERDC, Hanover, New Hampshire, USA.
[2]University of Alaska Fairbanks, Fairbanks, Alaska, USA.
[3]NOAA-PMEL, Seattle, Washington, USA.
[4]Jet Propulsion Laboratory, Pasadena, California, USA.

0148-0227/02/2000JC000477$09.00

developed by *Hibler* [1979] or one of its derivatives [e.g., *Semtner*, 1987; *Oberhuber*, 1993; *Pollard and Thompson*, 1994; *Bitz*, 1997; *Hunke and Dukowicz*, 1997; *Zhang and Hibler*, 1997; *Weatherly et al.*, 1997]. In the Hibler sea ice model the dynamics are governed by a momentum balance equation, where ice motion is considered a function of drift due to wind and ocean current stress at the ice surface, acceleration due to sea surface tilt, the Coriolis effect, and internal ice stress. Of these terms, the internal ice stress remains the most open-ended, since it has not been measured directly. Rather, it is determined by assuming a viscous-plastic rheology that relates the stress to deformation. Deformation, in turn, depends on an empirically defined ice strength, which is a function of the ice concentration and thickness. The ice strength is chosen by comparing model predictions of ice concentration and drift to data collected from drifting buoys and submarine-based ice thickness measurements. The recent ability to measure in-situ stress and to determine regional deformation from satellite imagery suggests that a more direct approach to evaluating the internal ice stress can be taken.

[5] Our ultimate goal is to use direct measurements to assist in the continued development and validation of sea ice dynamics models. As a step toward achieving that goal, we need to make a qualitative assessment of whether in-situ stress measurements are indeed related to the regional-scale (10–100 km) deformation behavior of the ice cover. This step is the focus of this paper.

[6] The work presented here builds on results from a previous experiment, conducted as part of the Sea Ice Mechanics Initiative (SIMI) [*Richter-Menge and Elder*, 1998]. The SIMI experiment was held from October 1993 to April 1994 in the Alaskan Beaufort Sea. During the SIMI field experiment, we deployed sensors to make direct measurements of the internal ice stress and position buoys to measure ice motion. Analysis of the deformation measurements made during SIMI demonstrated the granular plastic behavior of the sea ice [*Overland et al.*, 1998a]. A comparison of stress measurements made at several sites on a single multiyear floe provided insight on the sources and characteristics of internal ice stress in this region of the Arctic [*Richter-Menge and Elder*, 1998].

[7] The Surface Heat Budget of the Arctic Ocean (SHEBA) field experiment [*Perovich et al.*, 1999] provided another opportunity to collect data on ice stress and deformation. Stress sensors were used, again, to make direct measurements of the internal ice stress. Satellite coverage of the ice conditions during SHEBA was extensive. Therefore, satellite-derived ice motion products were used to assess the corresponding regional ice deformation. In this paper, these data are used to present four case studies, which represent winter sea ice conditions around Ice Station SHEBA. Each of these cases illustrates a different aspect of the ice behavior as it relates the physical environment. Together, these case studies confirm the general understanding of the process of ice dynamics and specifically illustrate the impact of coastal geometry and large-scale, sustained wind-forcing.

2. Data Sets

2.1. Stress Sensors

[8] Stress sensors were located on and around the multiyear floe that served as a base for Ice Station SHEBA. We used measurements from eight sensors in this study. All of these stress sensors were located near the top of the ice cover, at an average depth of 39 cm. The average ice thickness at these sites at the time of installation was 130 cm. Six of the sites were on the 3-km-diameter multiyear floe that served as a base for Ice Station SHEBA. These sites were arranged so that five of the sites were located at regular intervals along the edge of one quadrant of the floe, approximately 1 km apart. The other site on the main floe was located midway along this line of stress sensors, but 1 km toward the center of the floe. The remaining two sites were located on multiyear floes that were approximately 15 km from the ice station. All of the stress sensor sites were operational from 15 October 1997 through 1 April 1998, the period considered in this paper.

[9] The sensors used in the study were specifically designed for measuring in-situ ice stress [*Johnson and Cox*, 1982] and have been successfully used on a number of other arctic field experiments [*Johnson et al.*, 1985; *Tucker and Perovich*, 1992; *Richter-Menge and Elder*, 1998].

[10] Each sensor provides information on the stress acting at a point in the horizontal plane of the ice cover. Stresses are determined by measuring changes in the radial deformation of a cylindrical steel annulus, using a 120°, three-wire rosette. The wires in the rosette stretch across the hollow center of the annulus at the midpoint along its length. Periodically these wires are magnetically plucked to measure the frequency of vibration of each wire. Changes in the diameter of the annulus cause a change in the length of the wires and hence a change in the their frequency of vibration. Knowing the material properties of the steel annulus, we can directly relate this change in frequency to the stress applied to the sensor.

[11] Typically we use the data from the stress sensors to establish the primary (σ_1) and secondary principal (σ_2) stresses and the direction of the primary principal stress. We use the convention that compressive stresses are positive and that $\sigma_1 > \sigma_2$. Laboratory calibration tests, reported by *Cox and Johnson* [1983], indicated that over a loading range of 0 to 2 MPa the measured principal stress is within 15% of the applied stress and the principal stress direction is typically correct to within 5°. The tests also established that the resolution of the stress sensor is 20 kPa.

[12] In addition to measuring the ice stress, each sensor is equipped with a thermistor, providing the ice temperature at the point of the stress measurement.

[13] The stress sensors are frozen into the ice cover. They are installed in a 10-cm-diameter hole drilled through the ice cover, using standard coring equipment. A PVC pipe is attached to the end of the sensor so that it can be located downhole. The sensor is suspended at the desired depth by placing a cross bar, which rests on the ice surface, through the PVC pipe extension. Synchronized readings from all of the sensors were made throughout the SHEBA experiment at 5-min intervals.

[14] Under winter conditions in the central Arctic, there are two primary sources of stress: changes in the ice temperature and ice motion. As discussed by *Richter-Menge and Elder* [1998], the stress sensors cannot distinguish between these different sources of stress. In this paper, we are interested in making comparisons between the internal

Table 1. Correlation Coefficients Obtained From a Correlation Analysis of the Ice-Motion-Induced Stresses Measured Between 15 October 1997 and 1 May 1998 in the Vicinity of Ice Station SHEBA[a]

	Average	SHEBA 1	SHEBA 2	SHEBA 3	SHEBA 4	SHEBA 5	SHEBA 6	Floe 9	Floe 11
Average	1	0.78	0.45	0.61	0.53	0.54	0.69	0.79	0.80
SHEBA 1		1	0.18	0.32	0.35	0.25	0.51	0.67	0.63
SHEBA 2			1	0.22	0.07	0.21	0.34	0.26	0.21
SHEBA 3				1	0.31	0.34	0.34	0.35	0.46
SHEBA 4					1	0.08	0.30	0.32	0.24
SHEBA 5						1	0.37	0.31	0.45
SHEBA 6							1	0.42	0.42
Floe 9								1	0.66
Floe 11									1

[a] The time series between each of the eight different sites were compared, as well as the average stress of all of the sites to each of the individual sites.

ice stress and ice deformation. Therefore, it is necessary to isolate the stress caused by ice motion. Richter-Menge and Elder demonstrated, that, under winter conditions in the central Arctic, ice-motion-induced stresses can be estimated by subtracting the primary principal stress from the secondary principal stress ($\sigma_1 - \sigma_2$). This approach is based on the following observations: (1) ice-motion-induced stresses are highly directional, (2) changes in the ice temperature create stresses that are isotropic in the horizontal plane of the ice cover, and (3) changes in the ice temperature are strongly correlated with the secondary principal stress.

[15] We use the average of the ice-motion-induced stress measured at the different sites in our analysis, rather than any specific, individual site, because the average better represents the regional stress activity. Consistent with the results from the SIMI experiment [*Richter-Menge and Elder*, 1998], a comparison of the stress time history between individual SHEBA sites showed that, in general, there was a strong temporal correspondence in the stress activity at the different sites. This suggests that all of the sites were reacting to the same loading event. However, the specific characteristics of the stress at the individual sites, including the relative magnitude and the time of peak activity, showed significant spatial variability. We believe that the complex spatial variability reflects the influence of the ice thickness distribution, the dominant loading direction, and the proximity to local deformation activity.

[16] A correlation analysis of the time series of the internal ice stress between the various SHEBA sites provides a quantitative basis for this approach. The correlation coefficients between each pair of measurement sites and between the average stress and each measurement site are given in Table 1. Sites that were on the floe that served as the base for Ice Station SHEBA are labeled "SHEBA 1–6." Sites labeled "Floe 9" and "Floe 11" were on different multiyear ice floes, approximately 15 km from the SHEBA floe. In each case the correlation analysis was done over the period 15 October 1997 to 1 May 1998 using the raw stress signal. There is significant variation in the correlation coefficient between the individual sites, ranging from 0.07 (SHEBA 2: SHEBA 4) to 0.67 (SHEBA 1: Floe 9). Interestingly, the strongest correlation is between sites on different floes. The average correlation coefficient between the sites is 0.36 ± 0.15. The correlation between each of the measurement sites and the average stress is significantly stronger, averaging 0.65 ± 0.14. This analysis suggests that it would be difficult to choose any individual site record as being "the representative site" to compare to deformation measurements. On the other hand, an average of all of the stress records provides a good representation of the activity at each of the individual sites and, hence, a good representation of the overall characteristics of the internal ice stress in the vicinity of Ice Station SHEBA.

[17] Another measure of how well the average stress represents the stress activity at each of the individual sites is the standard error of the mean (SEM), defined as the standard deviation divided by the square root of the number of samples or, in this case, sites. Time series of the average internal ice stress and the standard error of the mean are presented in Figure 1a. The average internal ice stress varied significantly over the period 1 November 1997 to 1 April 1998, ranging from 0 to 60 kPa. The standard error of the mean exhibits significantly less variation over the same time period, averaging 4.2 ± 2.9 kPa. That the standard error of the mean shows relatively little increase during periods of significant stress activity suggests, again, that the average stress is a good representation of the regional internal ice stress.

2.2. Satellite Imagery Data

[18] This study uses two sources of satellite imagery data and two types of satellite-derived products. The RADARSAT SAR data were collected and processed at the Alaska SAR Facility (ASF) at the University of Alaska Fairbanks (UAF). The Thermal Infrared (TIR) data from the Advanced Very High Resolution Radiometer (AVHRR) on the NOAA-12 satellite were collected in near-real time at UAF and processed using the Terascan system and the Interactive Image Analysis System (IIAS) at ASF.

[19] The SAR data from RADARSAT can be obtained in multiple modes [*Ahmed et al.*, 1990]. For this study we use the ScanSAR-B wide-swath mode, which images an area approximately 460×512 km, covering incidence angles from 20 to 46.6° off nadir, with a resolution of 100 m. Our study includes both single-image SAR analyses as well as the use of image pairs. The SAR pairs were further processed using the SAR Geophysical Processor System (SGPS) at the Jet Propulsion Laboratory (JPL) [*Kwok et al.*, 1990]. The SGPS compares overlapping SAR scenes to create files of ice motion vectors sampled and plotted to a 5-km grid. Th e results are then combined in an along-track direction to provide a swath of continuous data. Since analyses are on a scene-by-scene basis, the SAR-derived ice motion products often display overlap between scenes along the swath, creating redundant vectors. This ensures data consistency along the track. The location of Ice Station

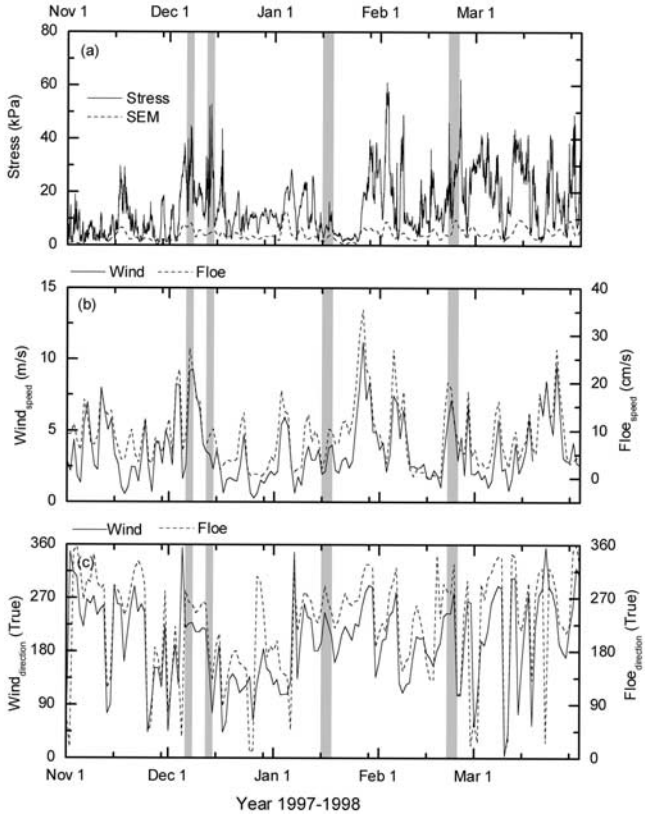

Figure 1. Time series of the (a) internal ice stress and the standard error of the mean (SEM), (b) surface wind speed and floe speed, and (c) wind direction and floe direction measured during SHEBA, from 1 November 1997 to 1 April 1998. The internal ice stress represents an average of the ice-motion-induced stress, estimated from measurements at eight different sites. The wind speed was measured 2 m above the ice surface. Both the wind and ice motion data are derived from measurements taken by the SHEBA Project Office at Ice Station SHEBA. The shaded bands denote the periods of our case studies.

SHEBA is shown as a star on the SAR-derived sea ice vector plots.

[20] The AVHRR data are from the NOAA-12 polar-orbiting satellite, whose characteristics are documented by *Kidwell* [1991]. This study used data from channel 4 (10.3–11.3 m), which is in the TIR range. The images selected are those most coincident in time with the overpasses of the SAR data collection, offering the best comparison of the data sets.

[21] The AVHRR images were oriented relative to the Alaska coastline using Terascan software. The AVHRR swath imaging characteristics are such that the size of the pixel increases across the swath away from nadir. In all cases we selected images that showed Ice Station SHEBA in the near- or midswath portion of the image to give us the highest resolution possible for comparison with the SAR data. The ice station location at the time of the satellite overpass is annotated on the images as a red cross.

[22] To compare the AVHRR and SAR images, an along-track mosaic of SAR images is registered to the same polar stenographic projection used to navigate the AVHRR. The data are then coregistered using ASF software to create a Hue-Lightness-Saturation (HLS) Composite [*Gleuck and Groves*, 1994]. For this technique the AVHRR TIR data were converted to surface temperature in °C using the Terascan software. No additional temperature correction was made, since we were not using the temperature values in an absolute sense for comparison to the SAR. The actual temperatures observed do include some clouds (shown as amorphous, warmer areas over the ice). We selected images that were cloud-free over Ice Station SHEBA.

[23] To create the composite, the higher-resolution SAR data are overlain on the AVHRR imagery. Values for the AVHRR data coincident with the SAR imagery are displayed using a color range that represents the values of the relative temperatures for each pixel. The maximum and minimum temperatures indicated on the color scale correspond to the values for the entire image. In our case the color scale on the HLS composite ranges from red, for a maximum temperature of −8°C, to blue, for a minimum temperature of −40°C. The SAR data are assigned to a gray scale and represent backscatter intensity. Both the SAR and AVHRR are then displayed on a background showing the remaining AVHRR image as gray values, also corresponding to the relative temperatures in the image. The resulting HLS composite adds new information to both the SAR and AVHRR data: the SAR adds detail to the AVHRR imagery while the AVHRR indicates the warmer ice in the SAR data, thereby helping to differentiate thinner ice associated with the active regions.

3. Results

3.1. Ice Motion

[24] Ice Station SHEBA was established on 2 October 1997, approximately 500 km offshore in the Beaufort Sea. SHEBA was located in the Perennial Ice Zone (PIZ), near the boundary between the Seasonal Ice Zone (SIZ) and the PIZ. The SIZ is the area that contains open water or a relatively lower concentration of ice floes in summer. The PIZ is the region of the Arctic Basin that maintains a relatively high ice concentration (≥90%) throughout the annual cycle.

[25] The drift of Ice Station SHEBA from 1 November 1997 to 1 April 1998 is presented in Figure 2. During this period there was an overall westward drift of approximately 575 km. Between 1 November and 1 February, Ice Station SHEBA generally moved parallel to the northern Alaskan coast. There were two periods of significant southerly movement toward the coast during this time: 25 November to 5 December and 12 December to 5 January. On 1 February, Ice Station SHEBA was due north of Point Barrow, Alaska. While continuing to move westward during the next month, the rate of movement of the ice station slowed. At this point, Ice Station SHEBA was moving toward Wrangel Island, off the Siberian coast. Between 1 March and 15 March, the drift was northward. The rate of movement increased again from 15 March to 1 April, as the drift direction became northwesterly.

[26] As described by *Steele et al.* [1997], during the winter the ice movement occurs primarily in response to wind-forcing at the top surface of the ice cover. For

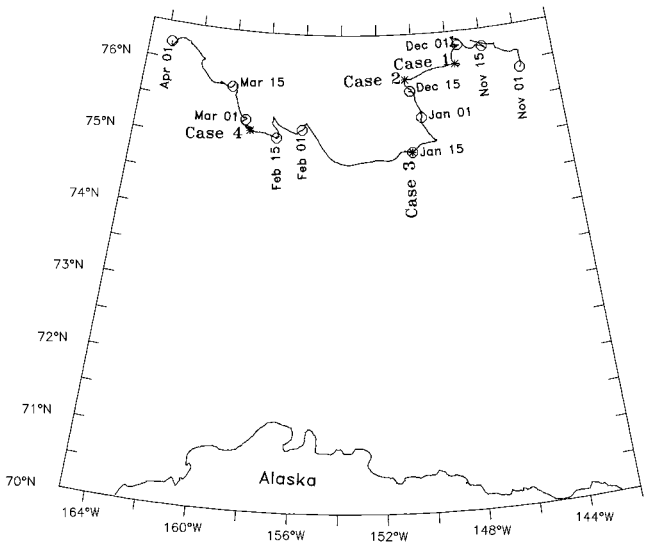

Figure 2. Drift of Ice Station SHEBA.

reference, time series of the wind speed and direction, measured at 2 m above the ice surface at Ice Station SHEBA from 1 November 1997 to 1 April 1998, are presented in Figures 1b and 1c. The corresponding speed and direction of the ice floe that served as a base for Ice Station SHEBA are also presented. All of these data are derived from measurements taken by the SHEBA Project Office and are available through their website: http://sheba.apl.washington.edu/. The wind direction describes the direction that the wind is blowing toward. While this is opposite of the convention normally adopted by meteorologists, it is more useful for comparing the wind direction to the direction of the ice movement. All of the time series represent daily averages of each measurement. The strong correspondence between the speed and the direction of the ice floe and the speed and direction of the surface wind is clearly evident. On average, the ratio between the speed of the ice floe and speed of the wind is 2.5%. The floe moved typically to the right of the wind, at an average angle of 33.7°.

3.2. Internal Ice Stress

[27] A time series of the average ice-motion-induced ice stress from the eight measurement sites between 1 November 1997 and 1 April 1998 is presented in Figure 1a. While data from the stress sensors were collected into June 1998, we have chosen this period because it coincides with the availability of satellite data at the time of this analysis. From November through mid-January, the characteristics of the internal ice stress are very similar to those observed during the SIMI program [*Richter-Menge and Elder*, 1998]. Most pronounced is the episodic nature of the stress signal. The sustained periods of relatively high stress (for example, 13–20 November and 3–12 December) are called stress events. These stress events last 3–10 days and exhibit both rapid and longer-duration changes in the magnitude of the stress. Based on our observations and the reports of others [*Johnson et al*, 1985; *Coon et al.*, 1989, 1998; *Comfort et al.*, 1992; *Tucker and Perovich*, 1992], the large and rapid changes in the stress are associated with the formation of ridges, leads, and rubble fields. These changes in stress happen on the order of hours and give the stress signal its spiky appearance. Underlying the rapid changes in the stress is a more gradual increase and, then, decrease in the stress. These longer-duration changes happen over a time period that is on the order of days. The similarity in the characteristics of the internal ice stress between SIMI and this period of the SHEBA experiment is not surprising. During this period Ice Station SHEBA was in the Alaskan Beaufort Sea, in nearly the same location as the SIMI experiment, and both were situated approximately 450–500 km offshore.

[28] Beginning in mid-January, there was a sustained period of low stresses. This period included nearly a week (19–25 January) when the internal ice stresses at all eight sites were close to zero. On 26 January, immediately following this period of extremely low stresses, there was a rapid increase in the stress. This increase in stress marked the beginning of an event that lasted 13 days, until 8 February. Immediately following this event, beginning on 12 February, there was a sequence of stress events, which appear linked by a gradual but marked increase in the underlying stress. Each of the individual events lasted around 3–5 days. The gradual increase in the stress lasted until 3 March, when the underlying stress gradually began to decrease. This record suggests that there was a 20-day period of relatively continuous compression of the ice cover. This is significantly longer than any of the loading periods observed earlier in the SHEBA

Table 2. Description of Four Representative Cases of Ice Conditions in the SHEBA Area of the Beaufort Sea and the Corresponding Internal Ice Stresses

Date	Ice Condition	Stress at Ice Station SHEBA
5–7 December 1997	Consolidation of the Seasonal Ice Zone (SIZ)	Large stress associated with local deformation
11–13 December 1997	Granular behavior of the SIZ; interaction with the Perennial Ice Zone (PIZ) boundary	Large regional stress pattern
14–17 January 1998	Divergence pattern; ice motion as a near-solid body	Little local or regional stress
20–23 February 1998	Basin-wide granular behavior; fracture and shear in the SIZ and PIZ	Very large, building stress event associated with leads opening off Wrangel Island and Siberian coast

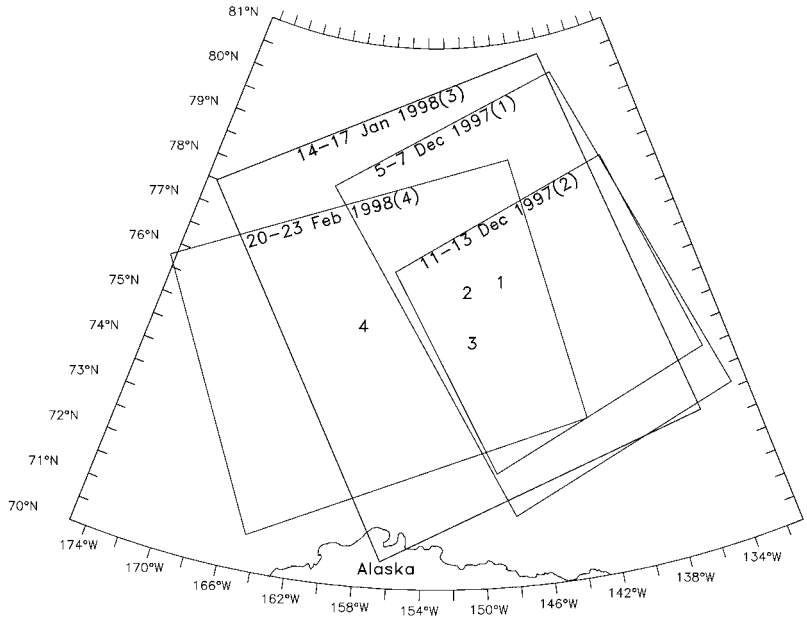

Figure 3. General region considered in the analysis of the satellite data, and the corresponding location of Ice Station SHEBA, for each case study. The SAR-derived swaths of ice motion are embedded within these regions.

stress time series or over the entire SIMI stress time series. This event was quickly followed by another 11-day event, from 9 March to 20 March. Another extended period of generally increasing ice stresses began on March 20 and lasted beyond the end of the record presented in this paper.

3.3. Ice Dynamics

[29] Based on the stress time series and the availability and quality of satellite-derived ice motion products, we selected four representative cases to investigate the relationship between ice stress and deformation under winter ice conditions: 5–7 December 1997, 11–13 December 1997, 14–17 January 1998, and 20–23 February 1998. The distinguishing characteristics of these time periods are summarized in Table 2. For reference, these periods are highlighted on the time series of internal ice stress, wind, and ice motion (Figure 1) and ice drift (Figure 2). Figure 3 illustrates the general region of the satellite data and the corresponding location of Ice Station SHEBA for each case. The SAR-derived swaths of ice motion, discussed later and shown in Figures 4, 5, 7, and 9, are located within these regions.

[30] The December cases consider two distinct periods of relatively high stress, which occurred during the same 15-day stress event. This event represents a period of consolidation soon after the ice cover had formed in the SIZ. According to ice charts, freeze-up of the SIZ in the fall of 1997 occurred in late November. Under these conditions, there was a continuous ice cover between the PIZ and Alaskan coast, but it was still relatively thin and unconsolidated.

[31] The peak stresses observed in the 5–7 December case began to develop on 3 December in response to a period of sustained, strong winds blowing toward the south-southwest. These winds, which began to develop on 1 December, pushed the ice toward the Alaskan coastline and initiated a period of consolidation in the SIZ. On 5 December there was an abrupt change in the direction of the ice drift, from south to west (Figure 2), as the component of the wind to the west increased. Figure 4 shows the SAR-derived sea ice displacements for 5–7 December 1997. Each vector in the image represents the actual displacement of the ice plotted every 10 km, as described earlier. There is a strong westerly component to all of the vectors, consistent with the shift to an overall westward drift of the ice cover. The magnitude of the motion is greater in the SIZ closest to the shore, with less motion farther offshore.

[32] Discontinuities in the characteristics of the motion vectors indicate differential motion within the pack, suggesting the location of narrow shear zones or sliplines. Between these sliplines the ice moved as an aggregate, with near solid body motion. The sliplines that are evident in Figure 4 were long, continuous features, which developed in and crossed the SIZ. The presence of the sliplines in the SIZ provides further evidence that the ice cover within this region was undergoing consolidation as it was forced against the coast by the sustained component of the winds to the south. The inset in Figure 4 shows the differential displacement velocities mapped using a 5-km grid. In this case the translation of the ice pack in the scene has been removed, and only the differential motion remains. Solid lines in the plots indicate transitions in the direction of the differential motion vectors. Ice Station SHEBA is, again, indicated by a star. The inset figure shows that the ice station was near a slipline, whose formation may be the reason for the sudden drop in stress on 6 December. The displacement anomalies in the smaller plot also show that the differential motion of the ice around SHEBA

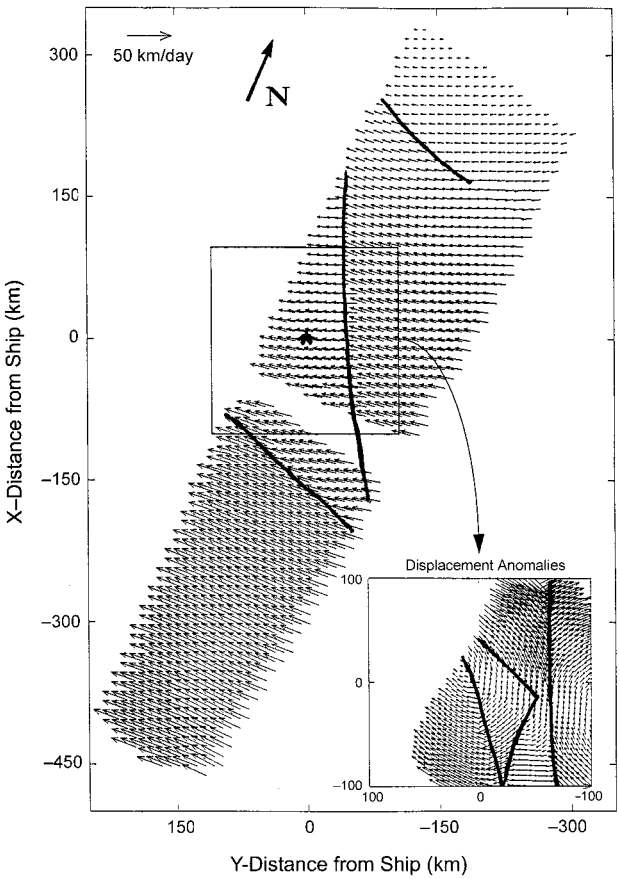

Figure 4. Displacement vectors from RADARSAT imagery for 5–7 December. The spacing of the vectors is 10 km, and solid lines represent shear or sliplines. Ice Station SHEBA is located at the star. The inset is the relative ice motion near Ice Station SHEBA, determined using a separate 5-km-grid data set. The solid lines represent sliplines, which, in this case, are likely to have formed when the ice was blown southward and compressed against the Alaskan coast just prior to this period.

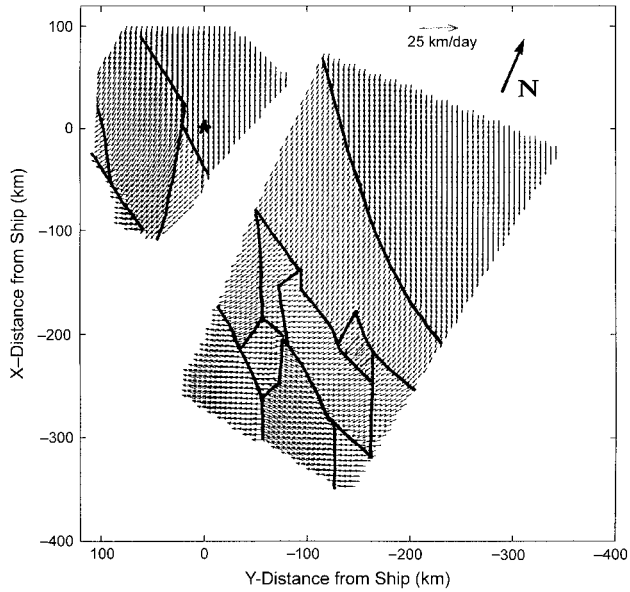

Figure 5. Displacement vectors for 11–13 December. Sliplines extend through the seasonal ice zone and into the perennial ice zone as the ice was, again, blown southward toward the Alaskan coast.

included a rotational component. This is consistent with the observation that there was an abrupt change in the direction of the general ice drift between 5 and 7 December, from south to west.

[33] The change in the direction of ice motion, which began on 5 December, initiated a 6-day period of westward movement (Figure 2). On 11 December the direction of the ice drift made another abrupt change, shifting from the west back to the south. This coincided with a change in the direction the wind was blowing, from south-southwest to south-southeast. The SAR-derived slipline field for 11–13 December is presented in Figure 5. Compared to the 5–7 December slipline field, there was significantly more shear deformation, occurring over a large area shoreward of SHEBA. In addition to the increased deformational activity near the shore, sliplines in the ice extended from the shore and throughout the SIZ into the edge of the PIZ. The magnitude of the motion vectors is more consistent over the entire region. While there is still

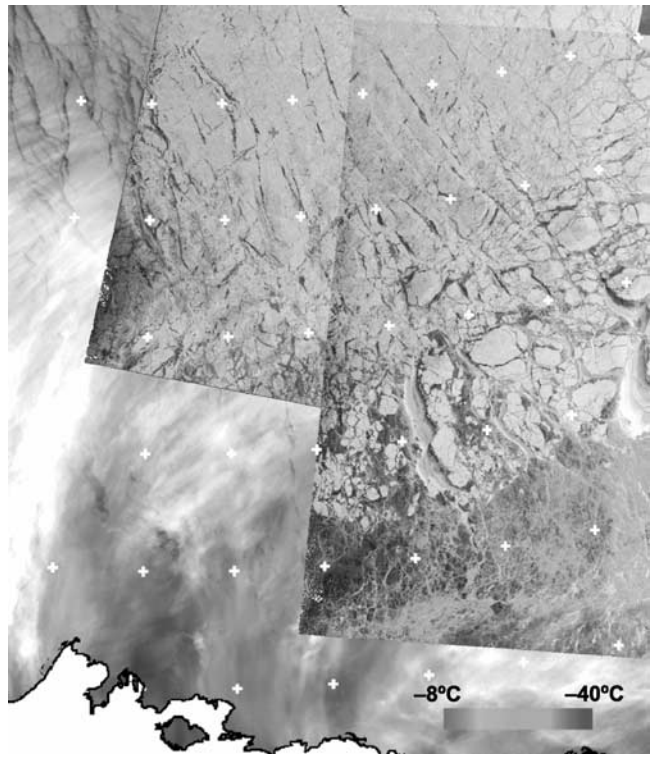

Figure 6. HLS composite [derived from SAR image with AVHRR temperature overlay (colors)] for 12 December 1997. Crosses are spaced at 1°-latitude by 5°-longitude intervals. The red cross is Ice Station SHEBA. See color version of this figure at back of this issue.

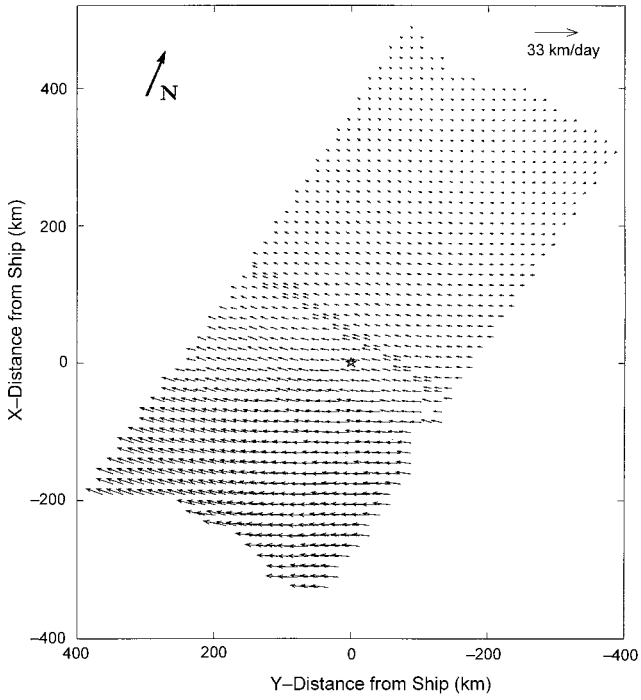

Figure 7. Displacement vectors for 14–17 January. The ice is diverging and no sliplines are evident.

a westward component to the vectors closer to the coastline, the vectors beyond the highly deformed region have a southerly component.

[34] Figure 6 shows an HLS composite for 12 December 1997. The location of Ice Station SHEBA is represented as a red cross on the AVHRR data. The color scale ranges from red, representing a maximum temperature of −8°C, to blue, representing a minimum temperature of −40°C. As described earlier, this composite is achieved by overlaying the SAR image on the TIR from the AVHRR. The SAR image alone can be difficult to interpret, but coupled with the HLS image, regions of significant activity become clear. The HLS composite shows warmer values in the areas with open water or thin ice, indicating active sliplines. Here the HLS composite shows the most active area of deformation to be shoreward of Ice Station SHEBA. The leads run throughout the SIZ to the edge of the PIZ and have a NNW-SSE and North-South orientation over the entire region. Each of these observations, derived from the HLS observations, supports the slipline interpretation from the SAR motion vectors in Figure 5.

[35] The 14–17 January case is distinguished by a period of extremely low average ice stress. Between 14 and 25 January the average stress was typically less than 10 kPa. For much of January, winds were fairly steady at a speed of about 4 m s^{-1} and predominantly blew toward the west. The ice in the SHEBA region responded to this surface wind stress by moving westward. The SAR-derived ice displacement vectors shown in Figure 7 for 14–17 January illustrate that the ice closest to the shore, in the region of the SIZ, advected more rapidly than the ice in the north. There are no sliplines observable in the SAR data. A comparison of the HLS composite for 14 January (Figure 8) with the 12 December composite (Figure 6) indicates that there was further opening of the ice cover in the region around Ice Station SHEBA. The most active area was east of Point Barrow. In the central and northern portion of the image, where SHEBA was located, there was no significant increase in the number of long, continuous shear lines. However, the highly dynamic area, characterized by smaller pieces of thick ice separated by large areas of thin ice, appears to have become more extensive, moving closer to SHEBA. This is clearly a period of ice divergence in the region near Ice Station SHEBA.

[36] The 20–23 February case occurred during a period when the stress activity was persistent, with an overall increase in the duration of the stress events (Figure 1a). Of the case studies we have selected, this case exhibits the most dramatic slipline pattern that developed near Ice Station SHEBA. At this time the general direction of ice movement was westward, toward Wrangel Island and the Siberian coast. Winds, which were toward the west, began to increase on 18 February, followed the next day by an increase in the ice stress. The SAR vectors for the SHEBA area for 20–23 February 1998 (Figure 9) show distinct sliplines (solid lines) and areas of convergence (dashed lines). In contrast to the January case the ice for the February case was most active away from the Alaskan coast. The ice near the coast, in the SIZ, remained relatively stable, while the ice farther offshore, near Ice Station SHEBA, moved westward as several aggregate plates.

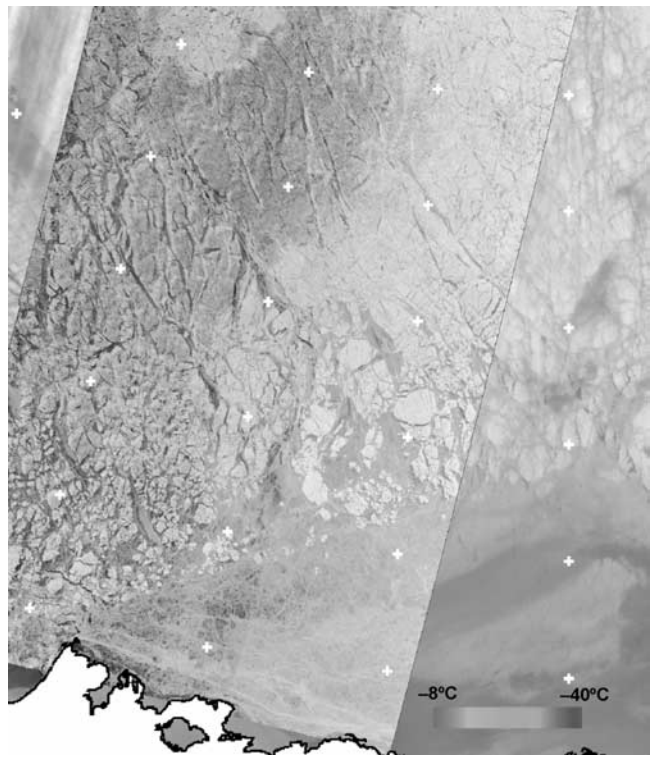

Figure 8. HLS composite for 14 January 1998. See color version of this figure at back of this issue.

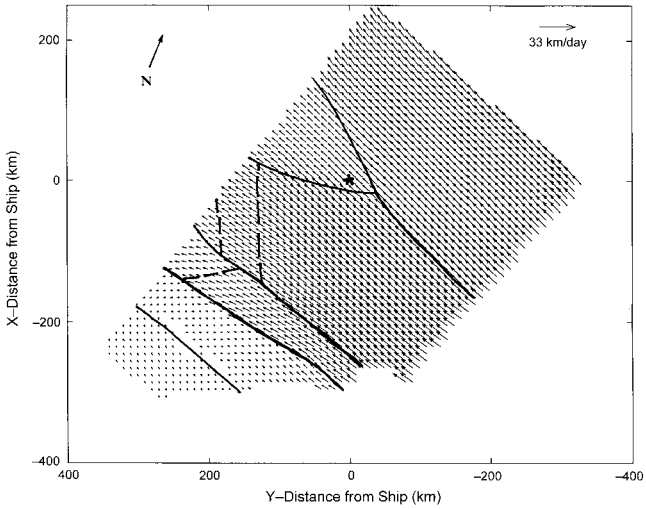

Figure 9. Displacement vectors for 20–23 February 1998. With sustained winds toward the west, the ice is blown westward, and a slipline pattern is established against Wrangel Island and the Siberian coast. The solid lines represent sliplines, and the dotted lines represent areas of convergence.

[37] An HLS composite for 18 February is presented in Figure 10, showing the condition of the ice pack just prior to 20–23 February in a region west of Ice Station SHEBA. This figure indicates the development of an extensive set of leads originating from Wrangel Island. Ice Station SHEBA lies just outside this lead system. In contrast to the December case, these leads were oriented away from the Siberian coastline and extended through the SIZ and well into the PIZ, up to 800 km away from Wrangel Island. This lead pattern appeared in less than a day. However, the stress data suggest that this fracture and failure in shear may have been building for several weeks. The formation of the lead system off Wrangel Island may have caused the rapid drop in the average ice stress observed between 16 and 18 February at Ice Station SHEBA (Figure 2a). While there was a rapid drop in the magnitude of the stress at this time, there was a continued, gradual increase in the underlying stress, which began in mid-February and continued into March. This suggests that, in the vicinity of Ice Station SHEBA, the ice was in a region of sustained compression, even during the formation of this large lead system to the north and west.

[38] Another, broader perspective on the ice dynamics during and between the 14–17 January and 20–23 February events is provided by an RGPS composite [*Kwok*, 1998] showing convergence and divergence and shear in the ice cover for 13–16 January, 25–28 January, and 15–18 February 1998 (Figure 11). Each frame in the RGPS composite shows the motion of the sea ice derived from SAR data, plotted on a 10-km-square grid. Changes in the perimeter and area of the samples are calculated, so the grids contain information as to the convergence or divergence of the ice, or the shear observed in the data set. There are no samples where the ice was heavily deformed, such as close to the coastlines, since the automated system has difficulty in tracking sea ice in these regions.

[39] Consistent with our earlier descriptions of significant divergence during the 14–17 January case, the 13–16 January 1998 frames indicate significant divergence along the Alaska coast (Figure 11, top left). This was accompanied by convergence of the ice in the Chukchi Sea, as it moved westward and piled up against the Siberian coast and Wrangel Island. The corresponding plot of the shear (Figure 11, top right) shows that the shear lines were closely associated with regions of convergence and divergence and were heaviest along the Alaskan coast. Winds during this period had a sustained component to the west, significantly increasing in speed during the end of January and the beginning of February (Figure 1b). The response of the ice cover to the increased magnitude of the wind-forcing is reflected in the 25–28 January 1998 frames of the RGPS composite. The divergence and shear north of the Alaska coast became more widespread, and there was increased convergence in the Chukchi Sea (Figure 11, middle left). Concurrently the length of the shear features increased dramatically (Figure 11, middle right). By 15–18 February there were only remnants of the highly dynamic features. The large shearline east of Wrangel Island can clearly be seen as a divergent feature in the two RGPS plots, while the surrounding ice remained relatively undeformed. At this point the ice had became less mobile, even though the wind continued to blow toward the west, albeit at a reduced speed. We believe that the redistribution of the ice contributed to this decrease in the deformation features, due to the increase in the ice strength caused by thickening. This explanation is consistent with the gradual increase in the internal ice stress observed during the latter part of February (Figure 1a).

4. Discussion

[40] These cases demonstrate that the internal ice stress measured during the SHEBA field experiment is related to regional ice deformation. In considering the implications of

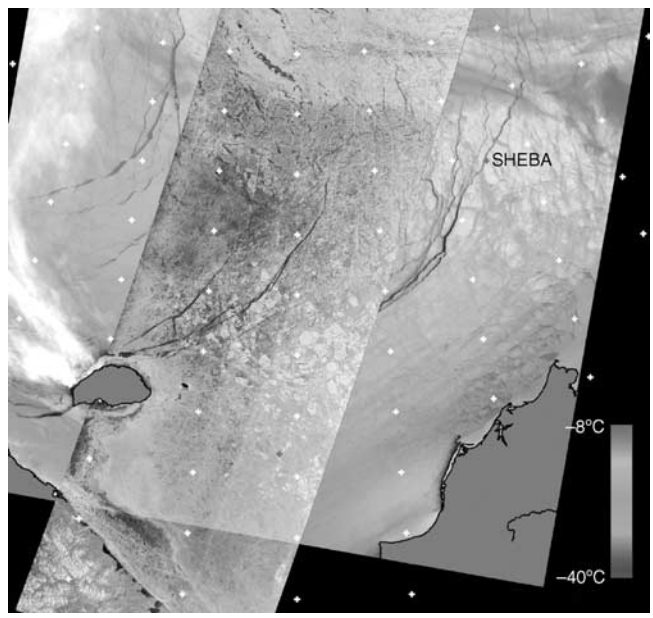

Figure 10. HLS composite for 18 February 1998. See color version of this figure at back of this issue.

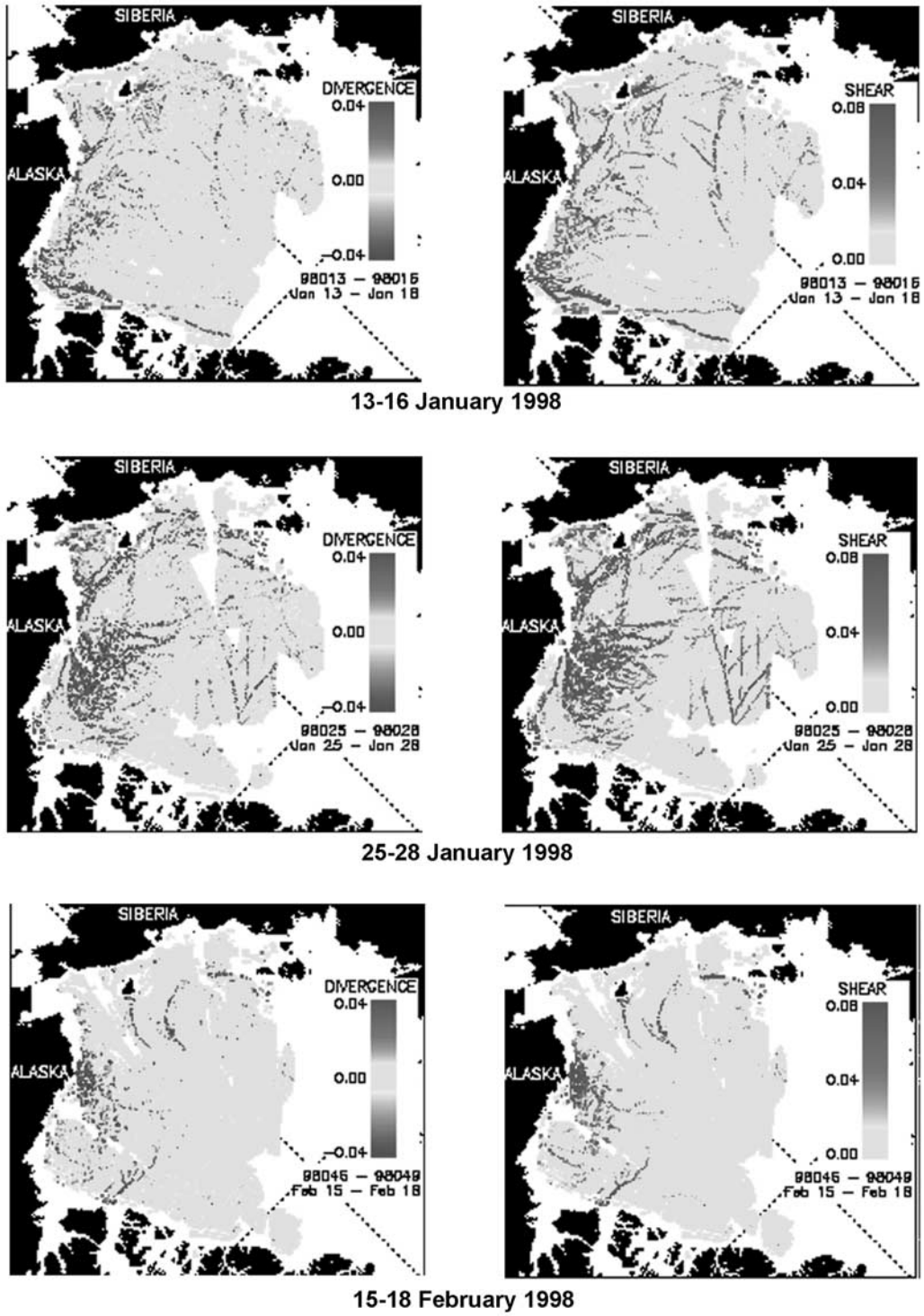

Figure 11. RGPS composite showing convergence and divergence (left column) and shear (right column) in the ice cover for 13–15 January (top), 25–28 January (middle), and 15–18 February 1998 (bottom). See color version of this figure at back of this issue.

this result, it is important to remember that the source of the stress data is an average of individual point measurements of stress. This suggests that during the winter, stress measured at a point in the ice cover does not simply reflect local deformation activity. For instance, an increase in stress does not typically mean that a ridge is forming close to the stress sensor. Rather, an increase in stress is associated with the overall state of the ice cover. It is difficult to define the extent of the region influencing the stress measured at a given point. However, we make the following observations to give some sense of the spatial scale: (1) the compression of the ice against a coastal boundary was measured by

stresssensors that were over 500 km offshore, and (2) the mechanical continuity of the ice cover is apparent in the formation of the aggregate plates, which are on the order of 50–150 km.

[41] We believe that these observations provide further support to the hypothesis that, during the winter, the ice cover behaves as a granular hardening plastic [*Overland et al.*, 1998a]. This description acknowledges that the fundamental component of the ice pack is the multiyear floe. The system's plasticity is established by the interaction of the floes, which move together in aggregate plates separated by sliplines. Hardening occurs through the process of consolidation, which results in the removal of relatively weak areas in the ice cover due to local failure events. In other words, relatively thin areas of ice become incorporated into ridges and rubble fields. This results in an overall thickening of the ice cover and, hence, an increase in its strength. The process of hardening is evident in the stress time series (Figure 1a). During any given stress event, the stress signal is a combination of rapid changes in the stress magnitude (local failure) superimposed on a more gradual increase in stress (overall hardening). The observation of an increase of the strength of the ice cover due to thickening is also consistent with a fundamental assumption made in many sea ice dynamics models. These models typically define the ice strength as a function of ice concentration and thickness [e.g., *Hibler*, 1979].

[42] By design, Ice Station SHEBA was a drifting experimental station. This resulted in the collection of data sets that were Lagrangian in nature. For us, the advantage in this design is the opportunity to observe how the general characteristics of the regional internal ice stress and ice dynamics change as a function of location.

[43] The general westward winter drift experienced by Ice Station SHEBA is consistent with the general circulation patterns reported for the Arctic Basin and in particular the Beaufort Sea. These circulation patterns are a function of the predominant wind and ocean current directions. Early in the experiment, Ice Station SHEBA was due north of the Alaskan coast. In this region of the Arctic the prevailing wind and ocean current are to the west, which act together to move the ice westward, parallel to the coastal boundary. Significant internal ice stress develops when this dominant circulation pattern is interrupted by the introduction of a sustained winds with a strong component to the south. Unlike the prevailing winds to the west, the winds to the south are associated with specific, episodic meteorological events, which typically last for several days. During these periods of winds to the south, the ice cover is pushed against the coast, the ice begins to consolidate, and internal ice stresses increase. When the internal ice stresses reach a magnitude equivalent to the strength of the ice cover, the ice fails through the formation of lead and ridge systems. With continued winds, the region of consolidation and, hence, of the lead and ridge systems moves seaward from the coast. When the period of winds to the south comes to an end, the ice resumes its westward movement due to the influence of the prevailing winds to the west. With the ice once again moving along the coast, rather than against it, the internal stresses diminish. This scenario is illustrated by the episodic nature of the stress time series from November into January (Figure 1a). Stress events during this period lasted 3–10 days, consistent with the timescale of major synoptic events.

[44] Due to the continued westward drift of Ice Station SHEBA, in late January we observed a transition in the dominant coastal boundary affecting the regional ice dynamics. As the ice station moved past Point Barrow, the ice began to consolidate against Wrangel Island and the Siberian coast. In this region of the Arctic the prevailing wind and ocean current, which remain to the west, move the ice directly toward the coastal boundary, rather than along it. Hence, the process of ice consolidation in this region of the Arctic Basin is more continuous. As in the case of ice interacting with the Alaskan coast, the internal ice stress builds as the ice is forced against the Siberian coast and undergoes consolidation. The ice fails when the internal ice stress reaches the strength of the ice. However, the relative continuity of this process in this region of the Arctic results in a higher degree of consolidation of the ice cover. Failure typically occurs under a persistent compressive loading. This situation gives rise to dramatic failure events, with lead and ridge systems reaching far offshore, into the central pack. With each failure event the ice pack thickens and the overall strength of the ice cover increases. This transition is also apparent in the stress time series, with a change from episodic stress events to stresses that are nearly continuous beginning in late January. Once the internal ice stress begins to develop in late January, there is a general increase in the underlying stress level. These observations are, again, consistent with the behavior of a hardening plastic.

[45] The transition of the dominant coastal boundary influencing the ice dynamics in the region of Ice Station SHEBA was not immediate. Rather, as the ice moved off the Alaskan coast and toward the Siberian coast, there was a period where there was little resistance to the westerly drift of the ice cover, even when the wind had a strong and sustained component to the south (Figures 1b and 1c and 2, 12–25 January). In this region of the Arctic Basin there is no rigid coastal boundary to offer resistance against the movement of the ice cover. The continuity of the Alaskan coastal boundary is lost at Point Barrow, and the Siberian coast is too distant to cause regional consolidation. Under these conditions the internal ice stress is negligible, and wind forces can cause the ice to undergo significant divergence, even under winter ice conditions. Measurements of the ice velocity indicate that between 19 and 25 January, when the average internal ice stress was near zero (Figure 1a), the average rate of ice movement was about 15 km per day, with a maximum of 35 km per day. For comparison, the average rate of ice drift from 1 November to 1 April was approximately 8 km per day.

[46] At any given location the relationship between the internal ice stress and regional ice deformation also exhibits a temporal dependence. As described in *Overland et al.* [1998b], to achieve winter ice conditions in the Beaufort Sea, the SIZ must freeze in completely. Once the transition from fall to winter ice conditions has occurred, the ice can begin to interact with the coastline and exhibit a granular-plastic behavior on a regional to basin scale (100–500 km). This transition is made apparent by the December cases, shown by comparing the satellite-derived patterns of ice deformation between 5–7 December (Figure 4) and 11–13

December (Figures 5 and 6). When the ice cover in the SIZ has just formed, it must thicken before it can effectively transmit stresses across the boundary between the SIZ and the PIZ. Consolidation of the ice cover against the coastal boundary is an effective mechanism for thickening. During this early stage of consolidation, sliplines form within the SIZ but do not extend into the PIZ. While the process of consolidating the SIZ takes place, it is possible to get significant ice movement along the coast, even when there is a strong, persistent component of the wind against the coast. These characteristics are illustrated in the 5–7 December case (Figure 4). Evidence that the ice cover in the SIZ is continuing to undergo further consolidation while the ice motion vectors have an along-shore component is provided by the internal ice stress time series (Figure 1a). During the 5–7 December case the magnitude of the average stress reached a maximum of about 40 kPa. Shortly after the ice began to move westward, the stress dropped but maintained a relatively high magnitude of 20 kPa. This suggests a continued compression of the ice cover, albeit at a reduced level.

[47] Eventually the ice in the SIZ becomes much less mobile, and motion is primarily toward further consolidation. This stage is indicated by an increase in the internal ice stress (Figure 1a). At this point the boundary between the SIZ and the PIZ becomes relatively transparent with respect to the development of sliplines, and true winter ice conditions are achieved (Figure 5). Evidence that the transition to winter ice behavior had begun by mid-December in the region around Ice Station SHEBA is most clearly provided in the HLS composite of 12 December (Figure 6). This figure shows the continuity of deformation features across the boundary between the SIZ and the PIZ. A similar example was observed during SIMI (see plate 1 in the work of *Overland et al.* [1998a]).

[48] Given the complexity of the ice dynamics process, it is interesting to observe the consistency in the magnitude of the average internal ice stress that developed during the SHEBA experiment. Early in the season, when the ice cover in the SIZ was developing (Figure 1a, 1 October to 1 December), peak stresses during stress events were 20–30 kPa. After the transition to a winter ice cover (Figure 1a, 1 December), peak stresses increased to 30–50 kPa. Recent ice dynamic models studies have assumed that the ice compressive strength is on the order of 10 kPa [*Hunke and Dukowicz*, 1997; *Zhang and Hibler*, 1997]. While work remains in developing an understanding of how a point measurement of stress in an ice cover relates to the compressive strength assumed in models, it is encouraging to see that the two values are comparable.

5. Summary

[49] The results of this work give qualitative evidence of a relationship between internal ice stress measurements and ice deformation at the regional scale. During periods of ice convergence, the internal ice stress increases, and during periods of divergence, the internal ice stress decreases. This observation comes as no surprise; it reflects basic material properties and has been used as a fundamental element in the successful development of numerous sea ice dynamics models. The novel component to this work is a demonstration of the ability to observe this material behavior with direct measurements of internal ice stress and deformation.

[50] The direct measurements provide insight into the process of regional ice deformation. It becomes clear from the examples we have presented that the relationship between the internal ice stress and deformation is complex because of the effects of the state of the ice cover, coastal boundaries, and forcing conditions. In general, internal ice stresses develop in the winter ice cover when: 1) the seasonal ice cover has completely developed between the perennial ice and the coast, 2) moderate to high winds occur over a sustained period, at least 2–3 days, and 3) these winds drive the ice toward a coastal boundary. Consistent with the behavior of a granular hardening plastic, the internal ice stress builds until the ice cover fails, resulting in the development of lead and ridge systems. The extent of the failure region depends on the persistence of the forcing conditions. After the ice in the seasonal ice zone is compacted against the shore, ice stress propagates away from shore, and shear deformation can occur throughout the seasonal ice zone. For shear to occur through the seasonal ice zone and into the perennial ice zone, creating large fractures covering several hundreds of kilometers, there must be sustained wind-forcing conditions that last for several days to weeks. The event ends with a change in wind direction, and ice must adjust to the new prevailing conditions.

[51] While qualitative in nature, these observations are an important step toward using direct measurements in the development and evaluation of sea ice dynamics models. An ability to use direct measurements for model development would be especially useful in creating models with a high (10–20 km) spatial resolution [*Overland and Ukita*, 2000]. Intrinsic to a higher spatial resolution is the need for establishing a more detailed understanding of the processes that govern ice motion [*Overland et al.*, 1995]. In collaboration with other investigators, we are currently using the stress and deformation data from the SHEBA experiment to improve a discrete element representation of the ice cover [*Hopkins*, 1996]. With the discrete element model, direct comparisons can be made between model-generated ice stresses and field measurements. Likewise, detailed failure patterns, produced by the model, can be compared to those observed in satellite-derived ice motion products. We plan to continue to use the combination of SAR ice motions and HLS imagery. The areal coverage of RADARSAT, compared to the ERS-1, is significantly better. Using ERS-1 [*Overland et al.*, 1998a], we were limited to observing the existence of sliplines, while with RADARSAT we can follow entire systems of sliplines. Combined, these tools may provide an important advance in the level of confidence of model representations of ice motion at both the regional and basin scale.

[52] **Acknowledgments.** Measurements made during the Surface Heat Budget of the Arctic Ocean (SHEBA) field experiment serve as the foundation for this work. Therefore, we extend our gratitude to those who provided their time, energy, and expertise to make this remarkable field program a success. We are particularly indebted to the crew of the Canadian Coast Guard Icebreaker *Des Groseilliers* and the logistics crew from the Applied Physics Laboratory, University of Washington, for their tremendous support during the SHEBA field program. Bruce Elder and Kerry Claffey each made significant contributions by assisting in collecting,

processing, and analyzing the stress data. The reviews of this paper resulted in significant changes to the original manuscript, which have improved the clarity of our presentation and our perspective on our past and future work. For this we thank the diligent JGR reviewers, who included Jinro Ukita and Ron Lindsay. This work was completed with grants from the National Science Foundation and the Office of Naval Research.

References

Ahmed, S., S. L. McNutt, H. R. Warren, and D. L. Low, The new RADARSAT: A cooperative mission to develop global resources paper presented at 41st Congress of the International Astronautical Federation, Dresden, GDR, 6–12 Oct., 1990.

Arbetter, T. E., J. A. Curry, M. M. Holland, and J. A. Maslanik, Response of sea ice models to perturbations in surface heat flux, *Ann. Glaciol.*, *25*, 193–197, 1997.

Bitz, C. M., Model study of natural variability in the arctic climate, Ph.D. thesis, Univ. of Washington, Seattle, Wash., 199 pp., 1997.

Comfort, G., R. Ritch, and R. M. W. Frederking, Pack ice stress measurements, in *Proceedings of the Eleventh International Conference on Offshore Mechanics and Arctic Engineering*, edited by O. A. Ayorinde et al., vol. 4, pp. 245–253, Am. Soc. of Mech. Eng., New York, 1992.

Coon, M. D., P. A. Lau, S. H. Bailey, and B. J. Taylor, Observations of ice floe stress in the eastern Arctic, in *Proceedings of the 10th International Conference on Port and Ocean Engineering Under Arctic Conditions*, edited by K. B. E. Axelsson and L. A. Fransson, vol. 1, pp. 44–53, Univ. of Technol., Lulea, Sweden, 1989.

Coon, M. D., G. S. Knoke, and D. C. Echert, The architecture of an anisotropic elastic-plastic sea ice mechanics constitutive law, *J. Geophys. Res.*, *103*(C10), 21,915–21,925, 1998.

Cox, G. F. N., and J. B. Johnson, Stress measurements in ice, *CRREL Rep. 83–23*, USA Cold Regions Res. and Eng. Lab., Hanover, N. H., 1983.

Gleuck, M., and J. E. Groves, Use of the HLS color model as a technique for combining AVHRR and ERS-1 imagery to evaluate near-shore ice processes in the St. Lawrence Island polynya, in *Proceedings of the Third Circumpolar Symposium on Remote Sensing in Arctic Environments*, p. 25, Univ. of Alaska-Fairbanks, 1994.

Hibler, W. D., III, A dynamic thermodynamic sea ice model, *J. Phys. Oceanogr.*, *9*, 815–846, 1979.

Hibler, W. D., III, The role of sea ice dynamics in modeling CO_2 increases, in *Climate Processes and Climate Sensitivity, Geophys. Monogr. Ser.*, vol. 29, edited by J. E. Hansen and T. Takahashi, 238–253, AGU, Washington, D. C., 1984.

Holland, D. M., L. A. Mysak, D. K. Manak, and J. M. Oberhuber, Sensitivity study of a dynamic thermodynamic sea ice model, *J. Geophys. Res.*, *98*(C2), 2561–2586, 1993.

Hopkins, M. A., On the mesoscale interaction of lead ice and floes, *J. Geophys. Res.*, *101*(C8), 18,315–18,326, 1996.

Hunke, E. C., and J. K. Dukowicz, An elastic-viscous-plastic model for sea ice dynamics, *J. Phys. Oceanogr.*, *27*(9), 1849–1867, 1997.

Johnson, J. B., and G. F. N. Cox, Stress sensor particularly suited for elastic, plastic, and viscoelastic materials, United States Patent 4,346600, Aug. 31, 1982.

Johnson, J. B., G. F. N. Cox, and W. B. Tucker, Kadluk ice stress measurement program, in *Proceedings of the Eighth International Conference on Port and Ocean Engineering Under Arctic Conditions*, vol. 1, pp. 88–100, 1985.

Kidwell, K. B. (Ed.), NOAA Polar-Orbiter Users' Guide, *NOAA Tech. Rep.*, 224 pp., Natl. Oceanic and Atmos. Admin., Washington, D. C., 1991.

Kwok, R. J., The RADARSAT Geophysical Processor System, in *Analysis of SAR Data of the Polar Oceans*, edited by C. Tatsoulis and R. Kwok, 235–257, Springer-Verlag, New York, 1998.

Kwok, R. J., J. C. Curlander, R. McConnell, and S. S. Pang, An ice-motion tracking system at the Alaska SAR Facility, *IEEE J. Oceanic Eng.*, *15*, 44–54, 1990.

Maykut, G. A., Energy exchange over young sea ice in the Central Arctic, *J. Geophys. Res.*, *83*(C7), 3646–3658, 1978.

Maykut, G. A., and N. Untersteiner, Some results from a time dependent, thermodynamic model of sea ice, *J. Geophys. Res.*, *76*, 1550–1575, 1971.

Oberhuber, J. M., Simulation of the Atlantic circulation with a coupled sea ice-mixed layer-isopycnal general circulation model, Part I, Model description, *J. Phys. Oceanogr.*, *23*(5), 808–829, 1993.

Overland, J. E., and J. Ukita, Dynamics of arctic sea ice discussed at workshop, *Eos Trans. AGU*, *81*(28), 309, 314, July 11, 2000.

Overland, J. E., B. A. Walter, T. B. Curtin, and P. Turet, Hierarchy and sea-ice mechanics: A case study from the Beaufort Sea, *J. Geophys. Res.*, *100*, 4559–4571, 1995.

Overland, J. E., S. L. McNutt, S. Salo, J. E. Groves, and S. Li, Sea ice as a granular plastic, *J. Geophys. Res.*, *103*, 21,845–21,867, 1998a.

Overland, J. E., S. L. McNutt, J. Richter-Menge, B. C. Elder, S. Salo, and J. E. Groves, Regional atmospheric forcing and ice response during SHEBA, *Fifth Conference on Polar Meteorology and Oceanography*, pp. 443–445, Am. Meteorol Soc., Boston, Mass., 1998b.

Perovich, D. K. et al., Year on the ice gives climate insights, *Eos Trans. AGU*, *80*, 481, 485–486, 1999.

Pollard, D., and S. L. Thompson, Sea ice dynamics and CO_2 sensitivity in a global climate model, *Atmos. Ocean*, *32*(2), 449–467, 1994.

Richter-Menge, J., and B. C. Elder, Characteristics of pack ice stress in the Alaskan Beaufort Sea, *J. Geophys. Res.*, *103*, 21,817–21,829, 1998.

Rind, D., R. Healy, C. Parkinson, and D. Martinson, The role of sea ice in 2 $\times$ CO_2 climate model sensitivity, Part I, The total influence of sea ice thickness and extent, *J. Clim.*, *8*, 449–463, 1995.

Semtner, A. J., A numerical study of sea ice and ocean circulation in the Arctic, *J. Phys. Oceanogr.*, *17*(8), 1077–1099, 1987.

Steele, M., J. Zhang, D. Rothrock, and H. Stern, The force balance of sea ice in a numerical model of the Arctic Ocean, *J. Geophys. Res.*, *102*, 21,061–21,079, 1997.

Thorndike, A. S., D. A. Rothrock, G. A. Maykut, and R. Colony, The thickness distribution of sea ice, *J. Geophys. Res.*, *80*, 4501–4513, 1975.

Tucker, W. B., III, and D. K. Perovich, Stress measurements in drifting pack ice, *Cold Reg. Sci. Technol.*, *20*, 119–139, 1992.

Untersteiner, N., On the mass and heat budget of Arctic sea ice, *Arch. Meteorol., Geophys. Bioklimatol., Ser. A*, *12*, 151–182, 1961.

Washington, W. M., and G. A. Meehl, General circulation model CO_2 sensitivity experiments: Snow-sea ice albedo parameterizations and globally averaged surface air temperature, *Clim. Change*, *8*, 231–241, 1986.

Weatherly, J. W., T. W. Bettge, and W. M. Washington, Simulation of sea ice in the NCAR climate model system, *Ann. Glaciol.*, *25*, 107–110, 1997.

Zhang, J. L., and W. D. Hibler III, On an efficient numerical method for modeling sea ice dynamics, *J. Geophys. Res.*, *102*(C4), 8691–8702, 1997.

R. Kwok, Jet Propulsion Laboratory, Pasadena, CA 91109, USA.

S. L. McNutt, University of Alaska Fairbanks, Fairbanks, AK 99775, USA.

J. E. Overland, NOAA-PMEL, Seattle, WA 98115, USA.

J. A. Richter-Menge, CRREL-ERDC, 72 Lyme Road, Hanover, NH 03755, USA. (jrichtermenge@crrel.usace.army.mil)

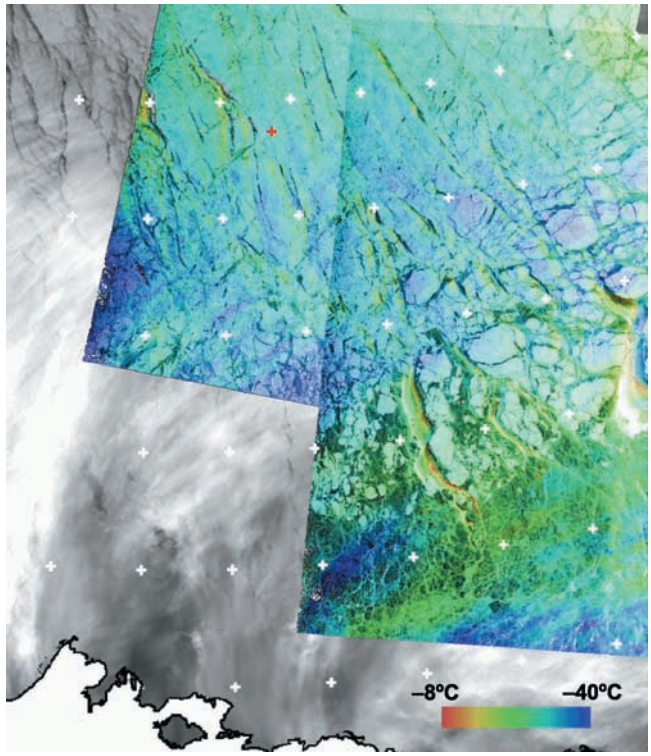

Figure 6. HLS composite [derived from SAR image with AVHRR temperature overlay (colors)] for 12 December 1997. Crosses are spaced at 1°-latitude by 5°-longitude intervals. The red cross is Ice Station SHEBA.

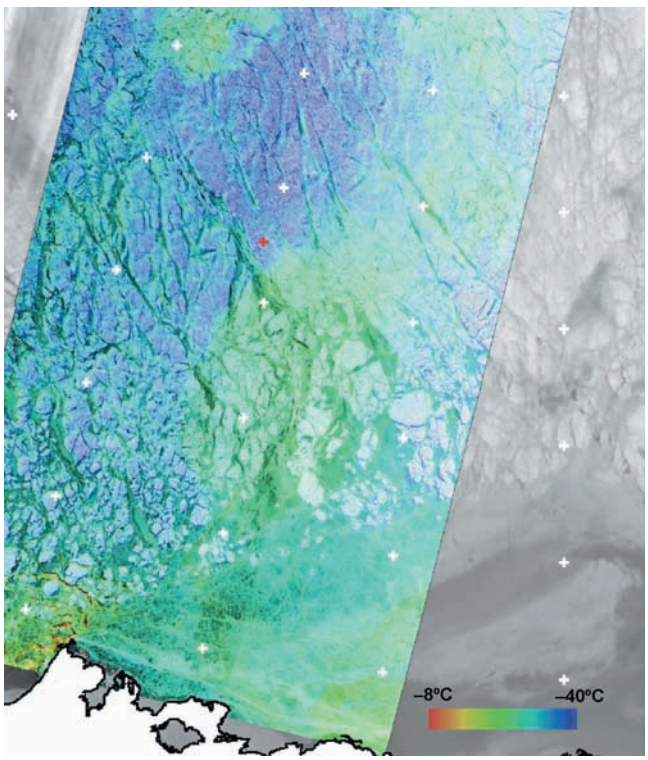

Figure 8. HLS composite for 14 January 1998.

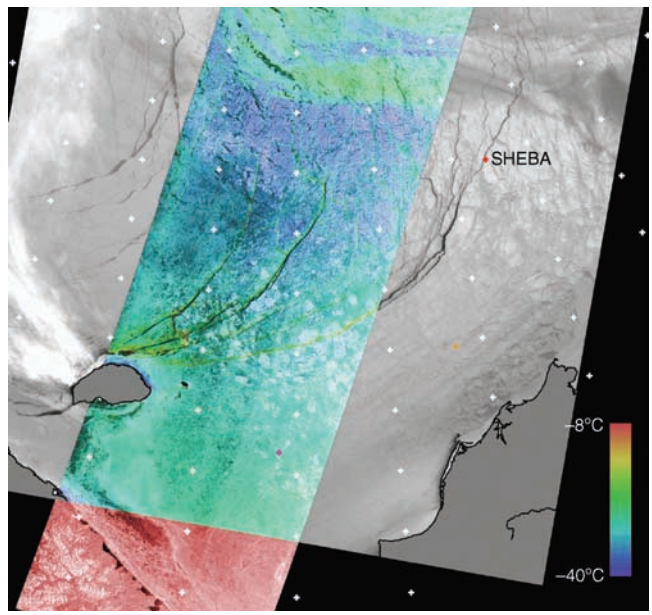

Figure 10. HLS composite for 18 February 1998.

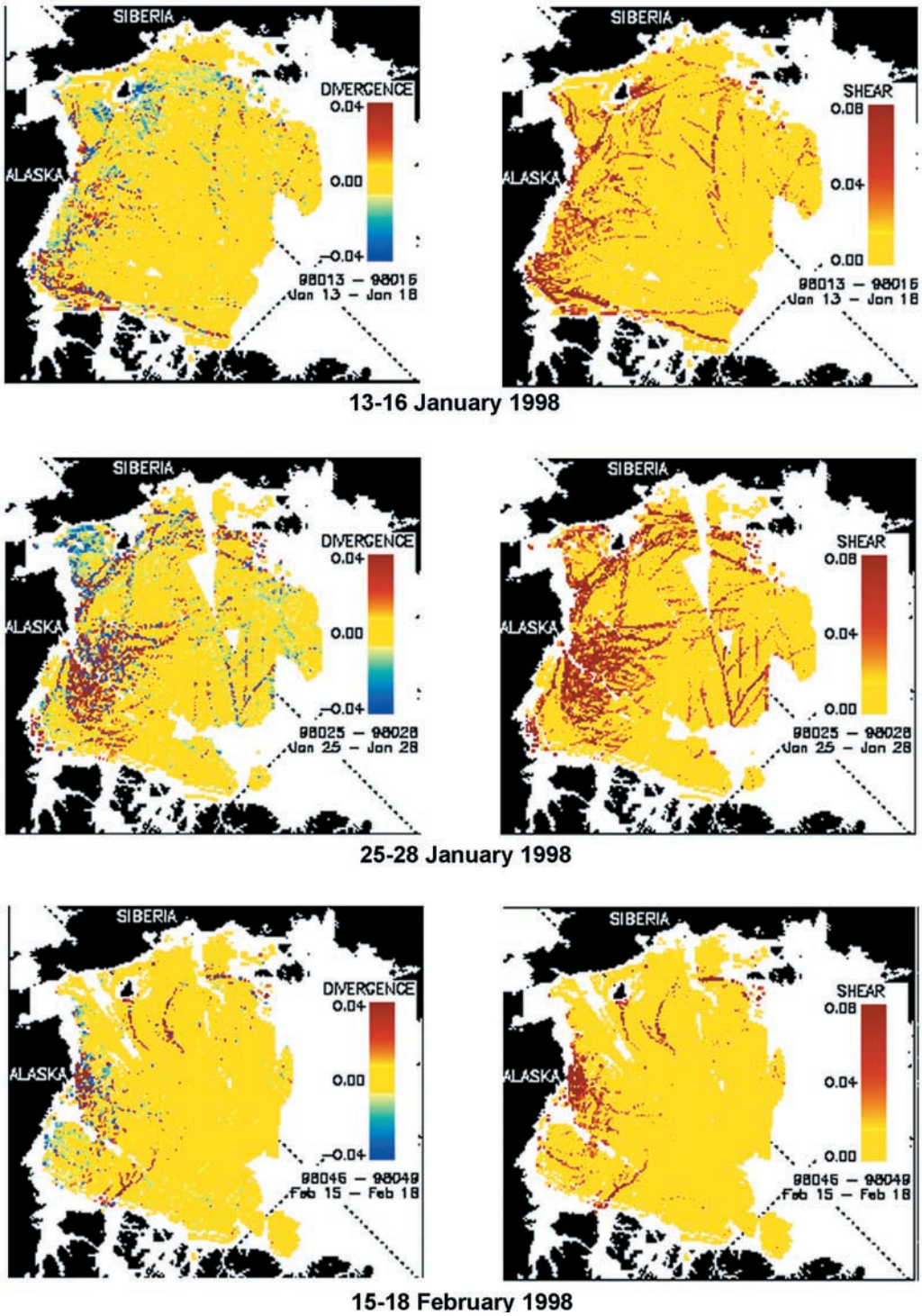

Figure 11. RGPS composite showing convergence and divergence (left column) and shear (right column) in the ice cover for 13–15 January (top), 25–28 January (middle), and 15–18 February 1998 (bottom).